Geophysical Journal International

Geophys. J. Int. (2017) **210,** 1176–1190
Advance Access publication 2017 May 26
GJI Gravity, geodesy and tides

doi: 10.1093/gji/ggx230

Analytical expressions for the gravitational vector field of a 3-D rectangular prism with density varying as an arbitrary-order polynomial function

Jianzhong Zhang[1,2] and Li Jiang[1]

[1]*Key Laboratory of Submarine Geosciences and Prospecting Techniques of the Ministry of Education, College of Marine Geosciences, Ocean University of China, Qingdao* 266100*, China. E-mail: zhangjz@ouc.edu.cn*
[2]*Evaluation and Detection Technology Laboratory of Marine Mineral Resources, Qingdao National Laboratory for Marine Science and Technology, Qingdao* 266061*, China*

Accepted 2017 May 25. Received 2017 May 22; in original form 2017 January 24

SUMMARY

The computation of gravitational vector field of variable-density bodies has been attracting much attention in high precision gravity investigation. In forward and inverse gravity modeling, a 3-D rectangular prism, as a simple building block, is commonly used to approximate 3-D variable-density bodies with irregular shape. In this paper, we first model the density of a rectangular prism using an arbitrary-order polynomial function of depth, and derive the closed-form expressions for computing the vertical and horizontal components of the gravitational vector field of a 3-D rectangular prism with the polynomial density variation. Then, we extend the polynomial density function of depth to a linear combination of three arbitrary-order polynomial functions in *x*-, *y*- and *z*-directions, and derive the analytical expressions of the gravitational vector field of a 3-D rectangular prism with such more general density function. The analytic expressions are numerically validated and compared with other existing methods. It is shown that the new expressions are far superior to the common method based on the stack of a collection of uniform subprisms in computational efficiency. In addition, the numerical error of the expressions is analysed and the results show that the expressions are available for practical applications.

Key words: Geopotential theory; Gravity anomalies and Earth structure; Numerical modelling.

1 INTRODUCTION

The calculation of the gravitational vector field of given mass bodies is a fundamental task in gravimetry and geodesy. One of the popular ways to calculate the gravitational vector field of irregular 3-D bodies is to approximate the bodies as a finite collection of 3-D rectangular prisms. The gravitational vector field of the bodies is then taken as an algebraic sum of the contributions of all rectangular prisms. Thus, the calculation of the gravitational vector field of a 3-D rectangular prism has an important role in both 3-D forward and inverse gravity problems. Mollweide (1813) first answered the vertical component of the gravitational vector field for a prism. Later Nagy (1966) and Banerjee & Das Gupta (1977) derived the closed-form expressions for the vertical component of the gravitational vector field of a vertical prism with constant density. Li & Chouteau (1998) reviewed the analytical algorithms for the gravitational field due to some regular-shaped bodies and listed the analytic expressions for the gravitational vector field of a 3-D rectangular prism with constant density. Nagy *et al*. (2000) presented the closed expressions of the gravitational potential and its vector and tensor fields for a prism with constant density.

In reality, most geological bodies have variable densities. For instance, Papp & Kalmar (1995) and Li (2001) demonstrated that the density of sediments increases with depth in their research basins. The density-log data in Verweij *et al.* (2016) showed that the density varies non-monotonically with depth at well E16–3 on the offshore Cleaverbank Platform in the Netherlands. It is relatively low at shallower depth, then increases with depth, and decreases at 2–3 km depth. Thereby, the interest has been increasing in gravitational vector field of a 3-D rectangular prism with variable density. Chai & Hinze (1988) derived a wavenumber-domain method for the vertical component of gravitational vector field of a vertical rectangular prism with density varying exponentially with depth. Later, several authors presented space-domain analytical expressions for the vertical component of gravitational vector field from a 3-D rectangular prism whose density varies with depth in a parabolic function (Chakravarthi *et al*. 2002), a quadratic polynomial function (Gallardo-Delgado *et al*. 2003) and

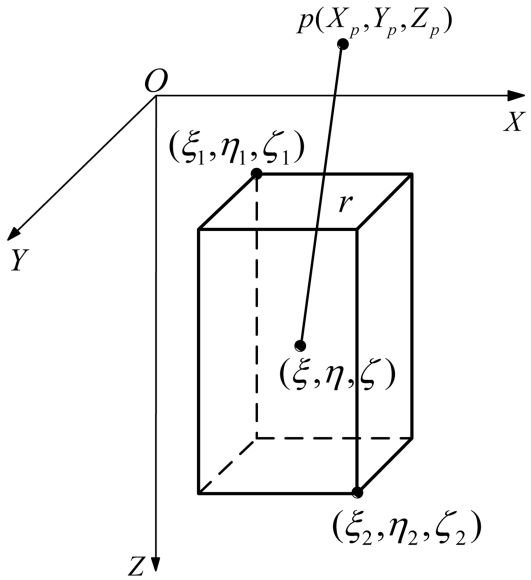

Figure 1. Geometrical definition of a 3-D rectangular prism.

a cubic polynomial function (García-Abdeslem 2005). Moreover, García-Abdeslem (1992) provided an analytical-numerical solution for calculating the vertical component of gravitational vector field generated by a vertical rectangular prism with a general depth-dependent density function, in which the 1-D integral with respect to depth was numerically evaluated. Zhou (2009) studied a semi-analytic method for the gravitational anomaly of a rectangular prism with density contrast varying in one or three directions, which reduced the 3-D volume integral of the gravitational anomaly equation to 1-D line integrals estimated by numerical method.

Zhang *et al*. (2001) first proposed any order polynomial density function varying with depth and lateral position, being flexible to describe the density variation of the real bodies. Zhang *et al*. (2001) and Zhou (2010), respectively, presented the closed-form expressions for vertical component of gravitational vector field from 2-D polygonal bodies with such variable density contrast. Wu & Chen (2016) developed a Fourier-domain method for computing the vector and tensor gravitational fields of 3-D prismatic bodies with variable density, in which the analytical spectrum of the gravitational vector field generated by a rectangular prism with polynomial depth-dependent density was obtained. Then, the inverse Fourier transform must be used on the spectrum of the gravitational vector field to obtain the gravitational vector field itself, and the truncation errors of this Fourier-domain method will be inevitable. In this paper, we derive the space-domain analytical expressions for the gravitational vector field of a 3-D rectangular prism whose density follows an arbitrary-order polynomial function of depth. By cyclic permutation of the *x*-, *y*- and *z*- coordinates, we obtain the analytical expressions for the gravitational vector field of a 3-D rectangular prism whose density varies as arbitrary-order polynomial functions in the three coordinate directions. The expressions are then validated using the analytic solution in García-Abdeslem (2005) and the popular method based on the stack of a collection of small uniform subprisms (Li & Chouteau 1998; Nagy *et al*. 2000).

2 EXPRESSION DERIVATIONS

2.1 Density varying with depth

For convenience, we adopt two right-handed Cartesian coordinate system: (X, Y, Z) for field coordinates and (ξ, η, ζ) for body coordinates. The vertical axes Z and ζ are taken to be positive downward, shown in Fig. 1. The vertical and horizontal components, U_z, U_x and U_y, of the gravitational attraction vector due to a 3-D rectangular prism with depth-dependent density $\rho(\zeta)$ at point $p(X_p, Y_p, Z_p)$ are (Lafehr & Nabighian 2012)

$$U_z(p) = G \iiint_V \frac{\rho(\zeta)(\zeta - Z_p)}{r^3} d\xi d\eta d\zeta, \tag{1}$$

$$U_x(p) = G \iiint_V \frac{\rho(\zeta)(\xi - X_p)}{r^3} d\xi d\eta d\zeta, \tag{2}$$

and

$$U_y(p) = G \iiint_V \frac{\rho(\zeta)(\eta - Y_p)}{r^3} d\xi d\eta d\zeta, \tag{3}$$

with

$$r = \sqrt{(\xi - X_p)^2 + (\eta - Y_p)^2 + (\zeta - Z_p)^2}, \tag{4}$$

where G is the universal gravitational constant and V is the volume of the prism. The prism is bounded by the planes $\xi = \xi_1, \xi = \xi_2, \eta = \eta_1, \eta = \eta_2, \zeta = \zeta_1$ and $\zeta = \zeta_2$.

For a mass body with depth-dependent density, the variation of the density can be described as an arbitrary-order polynomial function with depth (Zhang *et al*. 2001), which is able to accommodate a large variety of geological formations (D'Urso 2015). We express the density variation with depth for a 3-D rectangular prism as

$$\rho(\zeta) = \sum_{i=0}^{n} a_i \zeta^i, \tag{5}$$

an nth-order polynomial function with depth ζ. The constant coefficients a_i $(i = 0, 1, \ldots, n)$ can be found by fitting eq. (5) to the known density-depth data of a mass body, for example, sedimentary rocks.

Substituting the density function in eq. (5) into eqs (1)–(3) and invoking the following identity:

$$\zeta^i = (\zeta - Z_p + Z_p)^i = \sum_{j=0}^{i} C_i^j Z_p^{i-j} (\zeta - Z_p)^j, \tag{6}$$

where C_i^j is the binomial expansion coefficients, we rewrite eqs (1)–(3) as

$$U_z(p) = G \sum_{i=0}^{n} \sum_{j=0}^{i} a_i C_i^j Z_p^{i-j} \iiint_V \frac{z^{j+1}}{r^3} dxdydz, \tag{7}$$

$$U_x(p) = G \sum_{i=0}^{n} \sum_{j=0}^{i} a_i C_i^j Z_p^{i-j} \iiint_V \frac{z^j x}{r^3} dxdydz, \tag{8}$$

and

$$U_y(p) = G \sum_{i=0}^{n} \sum_{j=0}^{i} a_i C_i^j Z_p^{i-j} \iiint_V \frac{z^j y}{r^3} dxdydz, \tag{9}$$

where $r = \sqrt{x^2 + y^2 + z^2}$, $x = \xi - X_p$, $y = \eta - Y_p$ and $z = \zeta - Z_p$. Defining the indefinite integrals

$$Izz_j = \iiint \frac{z^{j+1}}{r^3} dxdydz, \tag{10}$$

$$Izx_j = \iiint \frac{z^j x}{r^3} dxdydz, \tag{11}$$

and

$$Izy_j = \iiint \frac{z^j y}{r^3} dxdydz, \tag{12}$$

where $j = 0, 1, \ldots, n$, the vertical and horizontal components of the gravitational vector field are, respectively,

$$U_z(p) = G \sum_{i=0}^{n} \sum_{j=0}^{i} a_i C_i^j Z_p^{i-j} Izz_j \Big|_{x_1}^{x_2} \Big|_{y_1}^{y_2} \Big|_{z_1}^{z_2}, \tag{13}$$

$$U_x(p) = G \sum_{i=0}^{n} \sum_{j=0}^{i} a_i C_i^j Z_p^{i-j} Izx_j \Big|_{x_1}^{x_2} \Big|_{y_1}^{y_2} \Big|_{z_1}^{z_2}, \tag{14}$$

and

$$U_y(p) = G \sum_{i=0}^{n} \sum_{j=0}^{i} a_i C_i^j Z_p^{i-j} Izy_j \Big|_{x_1}^{x_2} \Big|_{y_1}^{y_2} \Big|_{z_1}^{z_2}, \tag{15}$$

where $x_1 = \xi_1 - X_p$, $x_2 = \xi_2 - X_p$, $y_1 = \eta_1 - Y_p$, $y_2 = \eta_2 - Y_p$, $z_1 = \zeta_1 - Z_p$ and $z_2 = \zeta_2 - Z_p$.

The following focuses on considering the indefinite integrals in eqs (10)−(12). In the following indefinite integral equations, we omit the integral constants because the constant terms vanish in computing the definite integrals. First, we solve the indefinite integral in eq. (10). Integrating it with respect to x, we have

$$Izz_j = \iint \frac{xz^{j+1}}{(y^2 + z^2)r} dydz. \tag{16}$$

Applying eq. (A1) in the Appendix to integrate the integral in eq. (16) with respect to y and then using the partial-integration technique, we have

$$Izz_j = \frac{z^{j+1}}{j+1}\arctan\frac{xy}{zr} + \frac{xy}{j+1}\left[\int \frac{z^{j+1}}{(x^2+z^2)r}dz + \int \frac{z^{j+1}}{(y^2+z^2)r}dz\right]. \tag{17}$$

Let

$$\varphi_j(x,z) = \int \frac{z^{j+1}}{(x^2+z^2)r}dz, \tag{18}$$

we re-express eq. (17) as

$$Izz_j = \frac{z^{j+1}}{j+1}\arctan\frac{xy}{zr} + \frac{xy}{j+1}\left[\varphi_j(x,z) + \varphi_j(y,z)\right]. \tag{19}$$

Now we derive the solution of the indefinite integral of eq. (18) for two cases: j is even and j is odd.

Case 1: For j is even, let $j = 2\,m$ ($m = 0, 1, \ldots$), then

$$\varphi_j(x,z) = \int \frac{z^{2m+1}}{(x^2+z^2)r}dz = \frac{1}{2}\int \frac{z^{2m}}{(x^2+z^2)r}dz^2. \tag{20}$$

If $m = 0$ and $j = 0$, according to eq. (A4) in the Appendix, we have

$$\varphi_0(x,z) = \frac{1}{y}\left[\ln\sqrt{x^2+z^2} - \ln(y+r)\right]. \tag{21}$$

Exchanging x with y in eq. (21) yields $\varphi_0(y,z)$. From eq. (19) we then have

$$Izz_0 = z\arctan\frac{xy}{zr} - x\ln(y+r) - y\ln(x+r) + S, \tag{22}$$

where $S = x\ln\sqrt{x^2+z^2} + y\ln\sqrt{y^2+z^2}$. Since $x\ln\sqrt{x^2+z^2}$ and $y\ln\sqrt{y^2+z^2}$ are independent of y and x, respectively, definite integral $S\big|_{x_1}^{x_2}\big|_{y_1}^{y_2}\Big|_{z_1}^{z_2} = 0$. When substitute Izz_0 into eq. (13), S in eq. (22) vanishes.

If $m \geq 1$ and $j \geq 2$, applying the identity in eq. (6), eq. (20) becomes

$$\varphi_j(x,z) = \frac{1}{2}\int \frac{(x^2+z^2-x^2)^m}{(x^2+z^2)r}dz^2 = \frac{1}{2}\sum_{k=0}^{m} C_m^k(-1)^{m-k}x^{2(m-k)}\int \frac{(x^2+z^2)^{k-1}}{r}dz^2. \tag{23}$$

After applying eq. (A3) in the Appendix, we get

$$\varphi_j(x,z) = \frac{(-1)^m x^{2m}}{2y}\ln\frac{r-y}{r+y} + (-1)^{m-1}m!r\sum_{k=1}^{m}\frac{x^{2(m-k)}y^{2(k-1)}}{(m-k)!k}\sum_{l=0}^{k-1}\frac{(-1)^l r^{2l}}{l!(k-l-1)!(2l+1)y^{2l}}. \tag{24}$$

Similarly, exchanging x with y in eq. (24) yields $\varphi_j(y,z)$. And from eq. (19) we have

$$\begin{aligned} Izz_j = {} & \frac{z^{j+1}}{j+1}\arctan\frac{xy}{zr} + \frac{(-1)^{j/2+1}}{j+1}\left[x^{j+1}\ln(y+r) + y^{j+1}\ln(x+r) + T\right] + \frac{(-1)^{j/2-1}(j/2)!r}{j+1} \\ & \times \sum_{k=1}^{j/2}\left[\frac{x^{j-2k+1}y^{2k-1}}{(j/2-k)!k}\sum_{l=0}^{k-1}\frac{(-1)^l r^{2l}}{l!(k-l-1)!(2l+1)y^{2l}} + \frac{x^{2k-1}y^{j-2k+1}}{(j/2-k)!k}\sum_{l=0}^{k-1}\frac{(-1)^l r^{2l}}{l!(k-l-1)!(2l+1)x^{2l}}\right], \end{aligned} \tag{25}$$

where $T = -x^{j+1}\ln\sqrt{x^2+z^2} - y^{j+1}\ln\sqrt{y^2+z^2}$. Similarly to S in eq. (22), T also vanishes in computing the gravitational vector field.

Case 2: For j is odd, let $j = 2\,m + 1$ ($m = 0, 1, \ldots$), then

$$\varphi_j(x,z) = \int \frac{z^{2m+2}}{(x^2+z^2)r}dz. \tag{26}$$

If $m = 0$ and $j = 1$, applying eqs (A1) and (A2) in the Appendix, we have

$$\varphi_1(x,z) = \int \frac{x^2+z^2-x^2}{(x^2+z^2)r}dz = \ln(z+r) - \frac{x}{y}\arctan\frac{yz}{xr}, \tag{27}$$

and

$$Izz_1 = xy\ln(z+r) - \frac{x^2}{2}\arctan\frac{yz}{xr} - \frac{y^2}{2}\arctan\frac{xz}{yr} + \frac{z^2}{2}\arctan\frac{xy}{zr}. \tag{28}$$

If $m \geq 1$ and $j \geq 3$, applying the identity in eq. (6), eq. (26) becomes

$$\varphi_j(x,z) = \int \frac{(x^2+z^2-x^2)^{m+1}}{(x^2+z^2)r}dz = \sum_{k=0}^{m+1} C_{m+1}^k (-x^2)^{m-k+1} \int \frac{(x^2+z^2)^{k-1}}{r}dz$$

$$= (-1)^{m+1}x^{2(m+1)} \int \frac{1}{(x^2+z^2)r}dz + (-1)^m x^{2m} \int \frac{1}{r}dz + \sum_{k=2}^{m+1}(-1)^{m-k+1} C_{m+1}^k x^{2m} \sum_{l=1}^{k-1} C_{k-1}^l x^{-2l} \int \frac{z^{2l}}{r}dz. \tag{29}$$

Applying eqs (A1), (A2) and (A5) in the Appendix, eq. (29) becomes

$$\varphi_j(x,z) = \frac{(-1)^{m+1}x^{2m+1}}{y} \arctan\frac{yz}{xr} + (-1)^m x^{2m}\ln(z+r) + \sum_{k=2}^{m+1}\frac{(-1)^{m-k+1}(m+1)!x^{2m}}{(m-k+1)!k}$$

$$\times \sum_{l=1}^{k-1} \frac{(-1)^l (2l)!(x^2+y^2)^l}{2^{2l}(l!)^3(k-l-1)!x^{2l}} \left[\ln(z+r) + r\sum_{q=1}^{l}\frac{(-1)^q 2^{2q-1} q!(q-1)!z^{2q-1}}{(2q)!(x^2+y^2)^q}\right]. \tag{30}$$

Similarly, exchanging x with y in eq. (30) yields $\varphi_j(y,z)$. And from eq. (19), we have

$$Izz_j = \frac{(-1)^v x^{j+1}}{j+1}\arctan\frac{yz}{xr} + \frac{(-1)^v y^{j+1}}{j+1}\arctan\frac{xz}{yr} + \frac{z^{j+1}}{j+1}\arctan\frac{xy}{zr}$$

$$+ \frac{(-1)^{v-1}(x^j y + x y^j)}{j+1}\ln(z+r) + \frac{xy}{j+1}\sum_{k=2}^{v}\frac{(-1)^{v-k}v!}{(v-k)!k}\sum_{l=1}^{k-1}\frac{(-1)^l(2l)!(x^2+y^2)^l(x^{j-2l-1}+y^{j-2l-1})}{2^{2l}(l!)^3(k-l-1)!}$$

$$\times \left[\ln(z+r) + r\sum_{q=1}^{l}\frac{(-1)^q q!(q-1)!(2z)^{2q-1}}{(2q)!(x^2+y^2)^q}\right], \tag{31}$$

where $v = (j+1)/2$.

Eqs (13), (22), (25), (28) and (31) are the analytical expressions for the vertical component, U_z, due to a 3-D rectangular prism with nth-order polynomial density function of depth.

Next, we solve the indefinite integral in eq. (11). Integrating it with respect to x, we have

$$Izx_j = -\iint \frac{z^j}{r}dydz. \tag{32}$$

Using eq. (A2) in the Appendix to integrate eq. (32) with respect to y, we have

$$Izx_j = -\int \ln(y+r)z^j dz. \tag{33}$$

Applying the partial-integration technique and eq. (18), we express eq. (33) as

$$Izx_j = -\frac{z^{j+1}}{j+1}\ln(y+r) + \frac{1}{j+1}\int \frac{z^{j+2}}{(y+r)r}dz$$

$$= -\frac{z^{j+1}}{j+1}\ln(y+r) - \frac{y}{j+1}\varphi_{j+1}(x,z) + D, \tag{34}$$

where $D = \frac{1}{j+1}\int \frac{z^{j+2}}{x^2+z^2}dz$. D is independent of y. Similarly to S in eq. (22), D also vanishes in computing the gravitational vector field and thus is ignored in the following equations. Then, substituting the solution of the indefinite integral $\varphi_j(x,z)$ derived above into eq. (34), we have the analytical expressions of Izx_j as

$$Izx_0 = -z\ln(y+r) - y\ln(z+r) + x\arctan\frac{yz}{xr}, \tag{35}$$

$$Izx_j = \frac{(-1)^v x^{j+1} - z^{j+1}}{j+1}\ln(y+r) + \frac{(-1)^v v! r}{j+1}\sum_{k=1}^{v}\frac{x^{2(v-k)}y^{2k-1}}{(v-k)!k}\sum_{l=0}^{k-1}\frac{(-1)^l r^{2l}}{l!(k-l-1)!(2l+1)y^{2l}}, \tag{36}$$

for j is odd and $j \geq 1$, where $v = (j+1)/2$, and

$$Izx_j = \frac{(-1)^{w+1}x^{j+1}}{j+1}\arctan\frac{yz}{xr} - \frac{z^{j+1}}{j+1}\ln(y+r) + \frac{(-1)^w x^j y}{j+1}\ln(z+r) - \frac{y}{j+1}$$

$$\times \sum_{k=2}^{w}\frac{(-1)^{w-k}w!x^j}{(w-k)!k}\sum_{l=1}^{k-1}\frac{(-1)^l(2l)!(x^2+y^2)^l}{2^{2l}(l!)^3(k-l-1)!x^{2l}}\left[\ln(z+r) + r\sum_{q=1}^{l}\frac{(-1)^q 2^{2q-1}q!(q-1)!z^{2q-1}}{(2q)!(x^2+y^2)^q}\right], \tag{37}$$

for j is even and $j \geq 2$, where $w = j/2 + 1$.

Table 1. The conditions for the indeterminate forms for the arctangent and logarithm functions.

Functions	Conditions
$\arctan \frac{xy}{zr}$	$x = z = 0$ or $y = z = 0$
$\arctan \frac{yz}{xr}$	$x = y = 0$ or $x = z = 0$
$\arctan \frac{xz}{yr}$	$x = y = 0$ or $y = z = 0$
$\ln(x + r)$	$y = z = 0$ and $x \leq 0$
$\ln(y + r)$	$x = z = 0$ and $y \leq 0$
$\ln(z + r)$	$x = y = 0$ and $z \leq 0$

Similar to the derivation for Izx_j, we have the analytic expressions of Izy_j as

$$Izy_0 = -z\ln(x+r) - x\ln(z+r) + y\arctan\frac{xz}{yr}, \tag{38}$$

$$Izy_j = \frac{(-1)^v y^{j+1} - z^{j+1}}{j+1}\ln(x+r) + \frac{(-1)^v v!r}{j+1}\sum_{k=1}^{v}\frac{x^{2k-1}y^{2(v-k)}}{(v-k)!k}\sum_{l=0}^{k-1}\frac{(-1)^l r^{2l}}{l!(k-l-1)!(2l+1)x^{2l}}, \tag{39}$$

for j is odd and $j \geq 1$, where $v = (j+1)/2$, and

$$\begin{aligned} Izy_j = {} & \frac{(-1)^{w+1}y^{j+1}}{j+1}\arctan\frac{xz}{yr} - \frac{z^{j+1}}{j+1}\ln(x+r) + \frac{(-1)^w xy^j}{j+1}\ln(z+r) - \frac{x}{j+1} \\ & \times\sum_{k=2}^{w}\frac{(-1)^{w-k}w!y^j}{(w-k)!k}\sum_{l=1}^{k-1}\frac{(-1)^l(2l)!(x^2+y^2)^l}{2^{2l}(l!)^3(k-l-1)!y^{2l}}\left[\ln(z+r) + r\sum_{q=1}^{l}\frac{(-1)^q 2^{2q-1}q!(q-1)!z^{2q-1}}{(2q)!(x^2+y^2)^q}\right], \end{aligned} \tag{40}$$

for j is even and $j \geq 2$, where $w = j/2 + 1$.

Eqs (14) and (35)–(37) are the analytical expressions for the x-component U_x and eqs (15) and (38)–(40) are those for the y-component U_y, generated by a 3-D rectangular prism, the density of which varies according to an nth-order polynomial of the depth. When $n = 0$, the analytical expressions can be reduced to eq. (25) for x-component and eq. (26) for y-component in Li & Chouteau (1998) for a 3-D constant-density prism.

The analytical expressions (13), (22), (25), (28) and (31) for the vertical component U_z can also be reduced to, respectively, eq. (8) in Li & Chouteau (1998) for constant density when $n = 0$, eq. (3) in Gallardo-Delgado *et al*. (2003) for quadratic polynomial density function when $n = 2$ and the results of García-Abdeslem (2005) for cubic polynomial density function when $n = 3$. So far, the third order is the highest order of polynomial function used in describing the density variation of a 3-D rectangular prism. Our analytical expressions generalize the existing solutions for the gravitational vector field of a 3-D prism.

Moreover, the numerical singularity problem (Tsoulis & Petrović 2001) arises in our analytical expressions when computation points are placed on the straight lines through any edge of the rectangular prism. In thus a case, computation points meet the conditions listed in Table 1, the arctangent functions $\arctan\frac{xy}{zr}$, $\arctan\frac{yz}{xr}$ and $\arctan\frac{xz}{yr}$ and natural logarithm functions $\ln(x+r)$, $\ln(y+r)$ and $\ln(z+r)$ in eqs (22), (25), (28), (31) and (35)–(40) are indeterminate, but the terms containing them have limiting values of zero. For example, when a computation point is located at a corner of the prism (e.g. $x_1 = y_1 = z_1 = 0$, $x_2 \neq 0$, $y_2 \neq 0$ and $z_2 \neq 0$), all the terms containing functions $\arctan\frac{x_1y_1}{z_1r}$, $\arctan\frac{y_1z_1}{x_1r}$, $\arctan\frac{x_1z_1}{y_1r}$, $\ln(x_1+r)$, $\ln(y_1+r)$ or $\ln(z_1+r)$ on the right-hand sides of eqs (13)–(15), (22), (25), (28), (31) and (35)–(40) are not defined but have a zero limit, such as

$$\lim_{(x_1,y_1,z_1)\to(0,0,0)} z_1\arctan\frac{x_1y_1}{z_1r} = 0, \tag{41}$$

$$\lim_{(x_1,y_1,z_1)\to(0,0,0)} x_1\ln(y_1+r) = 0. \tag{42}$$

So the numerical singularity problem can be solved by assigning zero to the terms showing the indeterminate characteristics in direct computations. In this way, the proposed analytical expressions for the gravitational vector field have no singularities in whole space.

2.2 Density varying with depth and horizontal positions

We extend the polynomial density function with depth to a more general form with depth and horizontal positions, expressed as

$$\rho(\xi,\eta,\zeta) = \sum_{i=0}^{n_z} a_i\zeta^i + \sum_{i=0}^{n_x} b_i\xi^i + \sum_{i=0}^{n_y} c_i\eta^i, \tag{43}$$

a linear combination of an n_xth-order polynomial with horizontal distance ξ, an n_yth-order polynomial with horizontal distance η and an n_zth-order polynomial with depth ζ. a_i $(i = 0, 1, \ldots, n_z)$, b_i $(i = 0, 1, \ldots, n_x)$ and c_i $(i = 0, 1, \ldots, n_y)$ are the constant coefficients of the three

polynomials. If $n_z = 0$, eq. (43) is the polynomial density function of horizontal positions, representing that the density of a 3-D rectangular prism only varies horizontally.

Substituting the density function in eq. (43) into eqs (1)–(3) and invoking the similar identities in eq. (6), the vertical and horizontal components, U_z, U_x and U_y, of gravitational vector of a 3-D rectangular prism with the variable density following eq. (43) at point $p(X_p, Y_p, Z_p)$ are written as

$$U_\beta(p) = G\sum_{i=0}^{n_x}\sum_{j=0}^{i} b_i C_i^j X_p^{i-j} \iiint_V \frac{x^j\beta}{r^3}dxdydz + G\sum_{i=0}^{n_y}\sum_{j=0}^{i} c_i C_i^j Y_p^{i-j} \iiint_V \frac{y^j\beta}{r^3}dxdydz$$
$$+ G\sum_{i=0}^{n_z}\sum_{j=0}^{i} a_i C_i^j Z_p^{i-j} \iiint_V \frac{z^j\beta}{r^3}dxdydz, (\beta = x, y, z), \tag{44}$$

where $r = \sqrt{x^2+y^2+z^2}$, $x = \xi - X_p$, $y = \eta - Y_p$ and $z = \zeta - Z_p$. Defining the indefinite integrals

$$I_{\alpha\beta_j} = \iiint \frac{\alpha^j\beta}{r^3}dxdydz, \quad (\alpha = x, y, z; \beta = x, y, z), \tag{45}$$

the vertical and horizontal components of the gravitational vector field in eq. (44) are expressed as

$$U_\beta(p) = G\left(\sum_{i=0}^{n_x}\sum_{j=0}^{i} b_i C_i^j X_p^{i-j} I_{x\beta_j} + \sum_{i=0}^{n_y}\sum_{j=0}^{i} c_i C_i^j Y_p^{i-j} I_{y\beta_j} + \sum_{i=0}^{n_z}\sum_{j=0}^{i} a_i C_i^j Z_p^{i-j} I_{z\beta_j}\right)\Bigg|_{x_1}^{x_2}\Bigg|_{y_1}^{y_2}\Bigg|_{z_1}^{z_2} \quad (\beta = x, y, z), \tag{46}$$

where $x_1 = \xi_1 - X_p$, $x_2 = \xi_2 - X_p$, $y_1 = \eta_1 - Y_p$, $y_2 = \eta_2 - Y_p$, $z_1 = \zeta_1 - Z_p$ and $z_2 = \zeta_2 - Z_p$.

According to the analytic expressions of Izz_j in eqs (22), (25), (28) and (31) and by cyclic permutation of the x-, y- and z-coordinates, we summarize the analytic expressions of Ixx_j, Iyy_j and Izz_j as

$$I_{\beta\beta_0} = \beta\arctan\frac{\chi\delta}{\beta r} - \chi\ln(\delta + r) - \delta\ln(\chi + r), \tag{47}$$

$$I_{\beta\beta_1} = \chi\delta\ln(\beta + r) - \frac{\chi^2}{2}\arctan\frac{\delta\beta}{\chi r} - \frac{\delta^2}{2}\arctan\frac{\chi\beta}{\delta r} + \frac{\beta^2}{2}\arctan\frac{\chi\delta}{\beta r}, \tag{48}$$

$$I_{\beta\beta_j} = \frac{\beta^{j+1}}{j+1}\arctan\frac{\chi\delta}{\beta r} + \frac{(-1)^{j/2+1}}{j+1}\left[\chi^{j+1}\ln(\delta + r) + \delta^{j+1}\ln(\chi + r)\right] + \frac{(-1)^{j/2-1}(j/2)!r}{j+1}$$
$$\times\sum_{k=1}^{j/2}\left[\frac{\chi^{j-2k+1}\delta^{2k-1}}{(j/2-k)!k}\sum_{l=0}^{k-1}\frac{(-1)^l r^{2l}}{l!(k-l-1)!(2l+1)\delta^{2l}} + \frac{\chi^{2k-1}\delta^{j-2k+1}}{(j/2-k)!k}\sum_{l=0}^{k-1}\frac{(-1)^l r^{2l}}{l!(k-l-1)!(2l+1)\chi^{2l}}\right], \quad \text{for even } j \text{ and } j \geq 2, \tag{49}$$

$$I_{\beta\beta_j} = \frac{\beta^{j+1}}{j+1}\arctan\frac{\chi\delta}{\beta r} + \frac{(-1)^v}{j+1}\left[\chi^{j+1}\arctan\frac{\delta\beta}{\chi r} + \delta^{j+1}\arctan\frac{\chi\beta}{\delta r} - (\chi^j\delta + \chi\delta^j)\ln(\beta + r)\right]$$
$$+\frac{\chi\delta}{j+1}\sum_{k=2}^{v}\frac{(-1)^{v-k}v!}{(v-k)!k}\sum_{l=1}^{k-1}\frac{(-1)^l(2l)!(\chi^2+\delta^2)^l(\chi^{j-2l-1}+\delta^{j-2l-1})}{2^{2l}(l!)^3(k-l-1)!}$$
$$\times\left[\ln(\beta + r) + r\sum_{q=1}^{l}\frac{(-1)^q q!(q-1)!(2\beta)^{2q-1}}{(2q)!(\chi^2+\delta^2)^q}\right], \quad \text{for odd } j \text{ and } j \geq 3, \tag{50}$$

where $v = (j+1)/2$. $\beta = z$, $\chi = x$ and $\delta = y$ for Izz_j; $\beta = x$, $\chi = z$ and $\delta = y$ for Ixx_j; and $\beta = y$, $\chi = x$ and $\delta = z$ for Iyy_j.

According to analytic expressions of Izx_j in eqs (35)–(37) and by cyclic permutation of the x-, y- and z-coordinates, we summarize the analytic expressions of Iyx_j, Izx_j, Ixy_j, Izy_j, Ixz_j and Iyz_j as

$$I_{\alpha\beta_0} = -\alpha\ln(\delta + r) - \delta\ln(\alpha + r) + \beta\arctan\frac{\delta\alpha}{\beta r}, \tag{51}$$

$$I_{\alpha\beta_j} = \frac{(-1)^v\beta^{j+1} - \alpha^{j+1}}{j+1}\ln(\delta + r) + \frac{(-1)^v v!r}{j+1}\sum_{k=1}^{v}\frac{\beta^{2(v-k)}\delta^{2k-1}}{(v-k)!k}\sum_{l=0}^{k-1}\frac{(-1)^l r^{2l}}{l!(k-l-1)!(2l+1)\delta^{2l}}, \quad \text{for odd } j \text{ and } j \geq 1, \tag{52}$$

$$I_{\alpha\beta_j} = \frac{(-1)^{w+1}\beta^{j+1}}{j+1}\arctan\frac{\delta\alpha}{\beta r} - \frac{\alpha^{j+1}}{j+1}\ln(\delta + r) + \frac{(-1)^w\beta^j\delta}{j+1}\ln(\alpha + r) - \frac{\delta}{j+1}$$
$$\times\sum_{k=2}^{w}\frac{(-1)^{w-k}w!\beta^j}{(w-k)!k}\sum_{l=1}^{k-1}\frac{(-1)^l(2l)!(\beta^2+\delta^2)^l}{2^{2l}(l!)^3(k-l-1)!\beta^{2l}}\left[\ln(\alpha + r) + r\sum_{q=1}^{l}\frac{(-1)^q 2^{2q-1}q!(q-1)!\alpha^{2q-1}}{(2q)!(\beta^2+\delta^2)^q}\right], \quad \text{for even } j \text{ and } j \geq 2, \tag{53}$$

where $v = (j+1)/2$, $w = j/2 + 1$, $\alpha = x, y, z$, $\beta = x, y, z$, $\delta = x, y, z$, and $\alpha \neq \beta \neq \delta$.

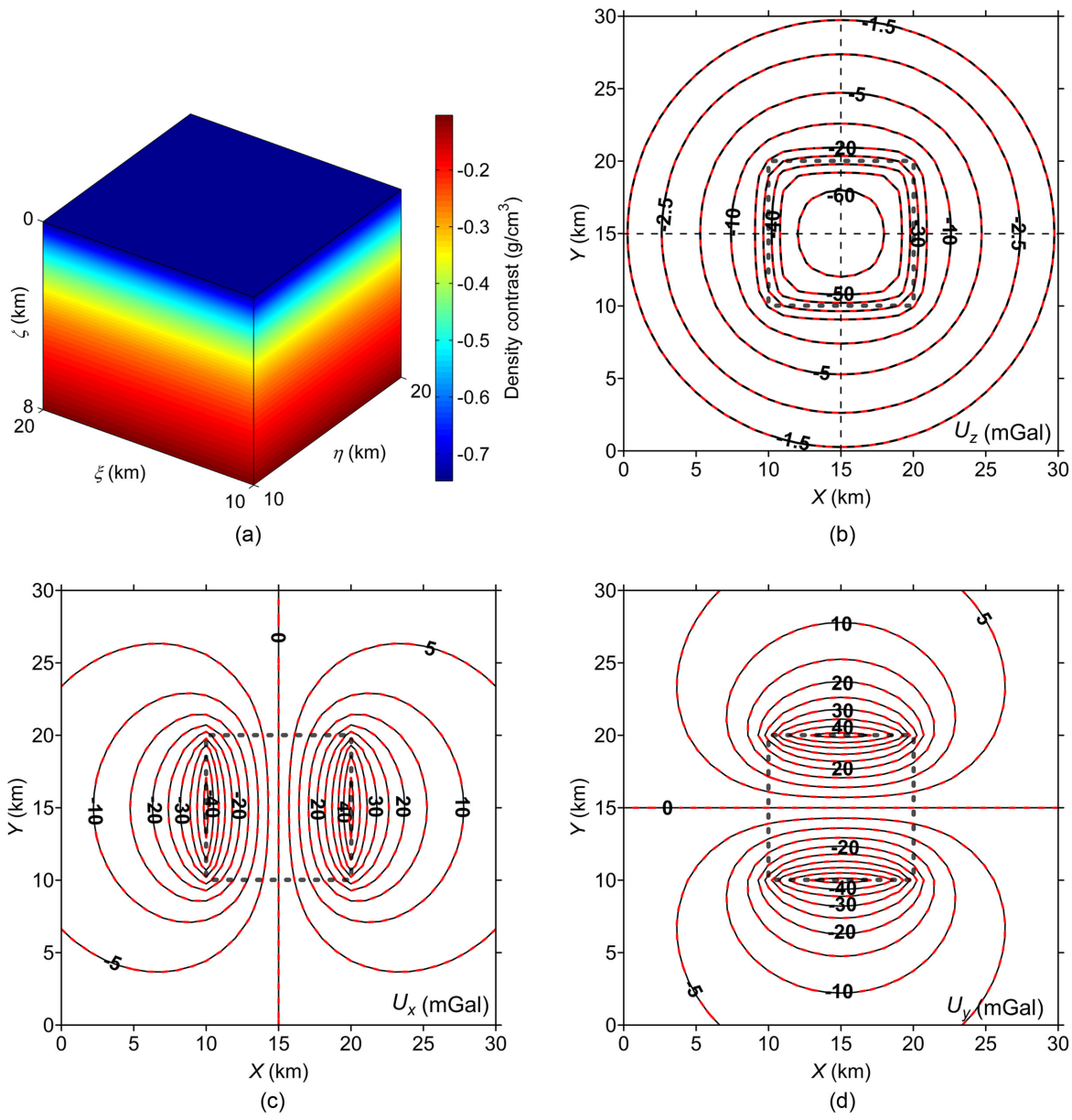

Figure 2. Gravitational vector field of the prism with cubic polynomial density contrast of depth given by eq. (54). (a) Prism model, (b) vertical component U_z, (c) x-component U_x and (d) y-component U_y. Solid lines indicate the field computed using the expressions proposed in this paper. Dashed ones in (b) indicate that using the analytic solution of García-Abdeslem (2005), and those in (c) and (d) indicate that using the method based on the stack of 35 uniform subprisms. The dotted rectangles indicate the projection of the edges of the prism on the computation plane.

Combining the analytical expressions in eqs (46)–(53), we can compute the horizontal components U_x and U_y and the vertical component U_z of the gravitational vector field of a 3-D rectangular prism with density varying vertically and horizontally. The numerical singularity of these analytical expressions in whole space can be tackled as mentioned above.

3 VALIDATION TESTS

In this section, we test the computation accuracy and efficiency of the analytic expressions derived in this paper. The prism model used here is the same as that in García-Abdeslem (2005), which extends from 10 to 20 km along the ξ- and η-directions, and from 0 to 8 km along the ζ-direction, shown in Fig. 2(a).The density contrast of the prism is considered to follow the polynomial functions of depth or of depth and horizontal positions. The computation points are placed at a 2-D grid on a plane coinciding with the top of the prism within a domain extending from 0 to 30 km along X- and Y-directions. 961 computation points are located on the grid, and the grid interval is 1 km in both X- and Y-directions. We compute the gravitational vector field of the prism with various density-contrast functions at the grid points applying, respectively, our analytical expressions proposed in this paper and the stack of a collection of uniform subprisms. The latter is a

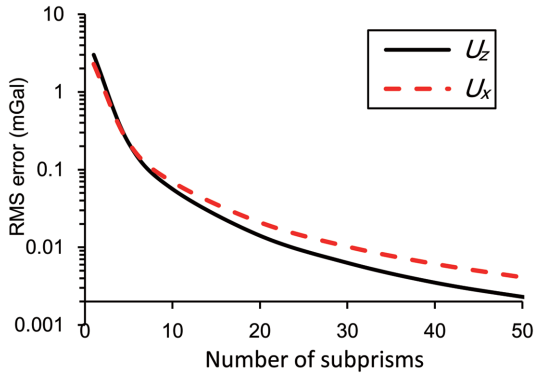

Figure 3. The rms errors between the gravitational vector field computed at 961 gridpoints using, respectively, the analytic expressions proposed in this paper and the method based on the stack of a collection of uniform subprisms versus the number of the subprisms. Solid line indicates the vertical component U_z, and dashed line the x-component U_x. Note that the line for y-component U_y is the same as that for U_x. The maximum rms error between them reaches about 3.00 mGal for U_z, 2.28 mGal for U_x and U_y for 1 subprism.

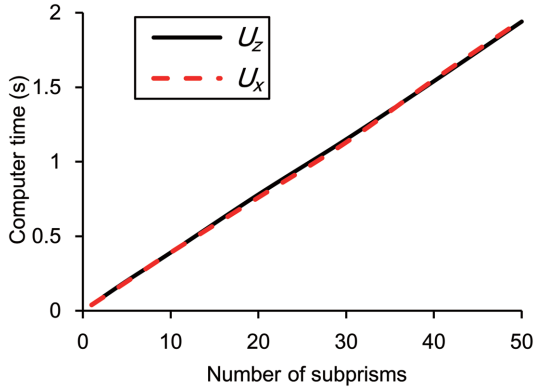

Figure 4. The computer time for computation of the gravitational vector field computed at 961 gridpoints using the method based on the stack of a collection of uniform subprisms versus the number of the subprisms. Solid line indicates the vertical component U_z, and dashed line the x-component U_x. Note that the line for y-component U_y is the same as that for U_x.

common method for 3-D variable-density bodies. All the computations are executed using MATLAB codes on a desktop computer with CPU of Intel(R) Core(TM) i5–2400 and Basic frequency 3.10 GHz, and RAM 4.00 GB.

3.1 Density varying with depth

The density contrast function used is the cubic polynomial of depth obtained by fitting the density-contrast data in Green Canyon in the Gulf of Mexico, given by García-Abdeslem (2005)

$$\Delta\rho(\zeta) = -0.7477 + 2.03435 \times 10^{-4}\zeta - 2.6764 \times 10^{-8}\zeta^2 + 1.4247 \times 10^{-12}\zeta^3, \tag{54}$$

where ζ is in metres and density contrast is in g cm^{-3}. First, we compute the gravitational vector field of the prism using our expressions where $n = 3$ and the vertical component of the gravitational vector field using the analytic solution of García-Abdeslem (2005), as shown in Fig. 2(b). The two results of the vertical components are completely consistent.

We also compute the gravitational vector field of the prism at the gridpoints using the stack of a collection of uniform subprisms. The prism is divided into a set of uniform subprisms along the ζ-direction. The constant density contrast of each subprism is assigned to the average of its density-contrast distribution. The gravitational vector field of each subprism is computed using the analytic expressions in Li & Chouteau (1998). Then, the gravitational vector field of the prism is obtained by summing the contributions of all uniform subprisms. The more the subprisms are, the more accurately the gravitational vector field is computed. Fig. 3 shows the rms errors between the gravitational vector field from our expressions when $n = 3$ and from the stack of uniform subprisms versus the number of the subprisms. We can see that the maximum rms error between them reaches about 3.00 mGal for U_z, 2.28 mGal for U_x and U_y when one subprism is used. When the number of the subprisms is larger than 35 the error is close to zero, and the results of the two methods are nearly the same. Figs 2(c) and (d) show that the horizontal components computed using our expressions and the stack of 35 uniform subprisms match well.

The CPU time used in performing our expressions for the each component is only 0.06 s or so. The CPU time in performing the stack of a collection of uniform subprisms for the each component increases nearly linearly with the number of the subprisms, as shown in Fig. 4. When the number of the subprisms is 35, the computational time for one component takes 1.37 s, about 21 times longer than ours. In order

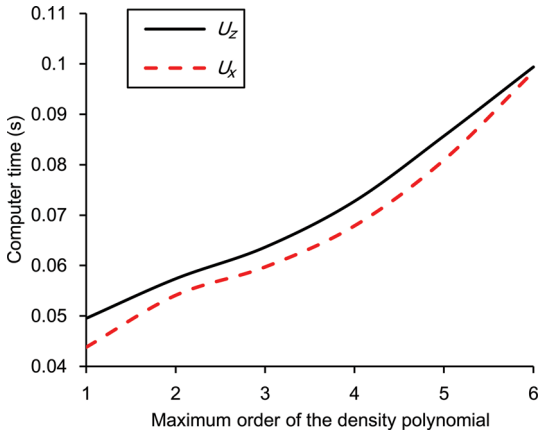

Figure 5. The computer time for computation of the gravitational vector field at 961 gridpoints using our analytic expressions versus the maximum order of the density polynomial. All the coefficients of the polynomial are 1. Solid line indicates the vertical component U_z, and dashed line the x-component U_x. Note that the line for y-component U_y is the same as that for U_x.

to achieve equivalent accuracy, the common method requires much more CPU time than ours. This example reveals that our expressions are superior to the common stack of uniform subprisms in terms of computational time in case of prismatic geometry.

In addition, the numerical complexity of our analytic expressions increases with the order of the density polynomial. Fig. 5 shows the CPU time for computing gravitational vector field of the prism model at 961 gridpoints using our expressions versus the maximum order of the density polynomial with coefficients of 1. The CPU time in performing our expressions depends on the maximum order of the density polynomial. The larger the maximum order is, the more the CPU time will be taken. The CPU time for the maximum order of 6 is about double that for the maximum order of 2. Therefore, the efficiency for computing the gravitational vector field using our expressions depends on both the number of prisms and the maximum order of the density polynomial in modelling a geological structure.

3.2 Density varying with depth and horizontal positions

To valid the analytical expressions derived above for the prism with horizontal and vertical density variations, we assign the prism to the same density-contrast function as that in Zhou (2009). The density contrast varies as a linear function in horizontal direction and a cubic polynomial function in depth, given by

$$\Delta\rho(\xi,\zeta) = -0.7477 + 2.03435\times10^{-4}\zeta - 2.6764\times10^{-8}\zeta^2 + 1.4247\times10^{-12}\zeta^3 - 2.32\times10^{-5}\xi, \tag{55}$$

where ξ and ζ are in metres and density contrast is in g cm^{-3}. The prism model is shown in Fig. 6(a). We compute the gravitational vector field of the prism using our expressions where $n_x = 1$, $n_y = 0$, $n_z = 3$ and the method based on the stack of uniform subprisms, respectively. For the latter method, the prism is divided uniformly into 35 segments along the ζ-direction and 16 segments along the ξ-direction, and 560 uniform subprisms are then obtained. Figs 6(b)–(d) show, respectively, the z-, x- and y-components, U_z, U_x and U_y, of the computed gravitational field. The each component is not symmetric in X-direction because of the horizontal density variation of the prism. The fields computed using the two methods agree very well with each other. The rms errors between them are about 0.01 mGal for U_z and U_x, and 0.0084 mGal for U_y. The computational time taken in performing our expressions for each component is only about 1.2 s, and that in performing the stack of 560 uniform subprisms for each component about 24 s, about 19 times longer than the former.

Another example involves the prism with the same geometry sizes as above prism but with density-contrast varying in all three directions. The density-contrast function is modelled as

$$\Delta\rho(\xi,\eta,\zeta) = -0.7477 + 2.03435\times10^{-4}\zeta - 2.6764\times10^{-8}\zeta^2 + 1.4247\times10^{-12}\zeta^3 - 8.0\times10^{-10}\xi^2 - 9.0\times10^{-10}\eta^2, \tag{56}$$

where ξ, η and ζ are in metres and density contrast is in g cm^{-3}. The gravitational vector field is computed using above two methods. For the method based on the stack of subprisms, the prism is divided uniformly into 30 segments along the ζ-direction, 10 segments along the ξ-direction and 10 segments along the η-direction, that is 3000 uniform subprisms. Figs 7(b)–(d) show that the three components of the field computed are unsymmetrical in both X- and Y-directions, reflecting the density variations of the prism in both ξ- and η-directions. The components of the vector field computed using our expressions where $n_x = 2$, $n_y = 2$ and $n_z = 3$ are consistent with those using the stack of 3000 uniform subprisms. The rms errors between the two computed fields are about 0.03 mGal for U_z, and 0.02 mGal for U_x and U_y. The computational time in performing our expressions for each component is only about 4.5 s, and that in performing the stack of 3000 uniform subprisms for each component about 142 s, about 30 times longer than the former. These examples show that our analytical expressions are more efficient in computing gravitational vector field of variable-density bodies than the common method based on the stack of uniform subprisms.

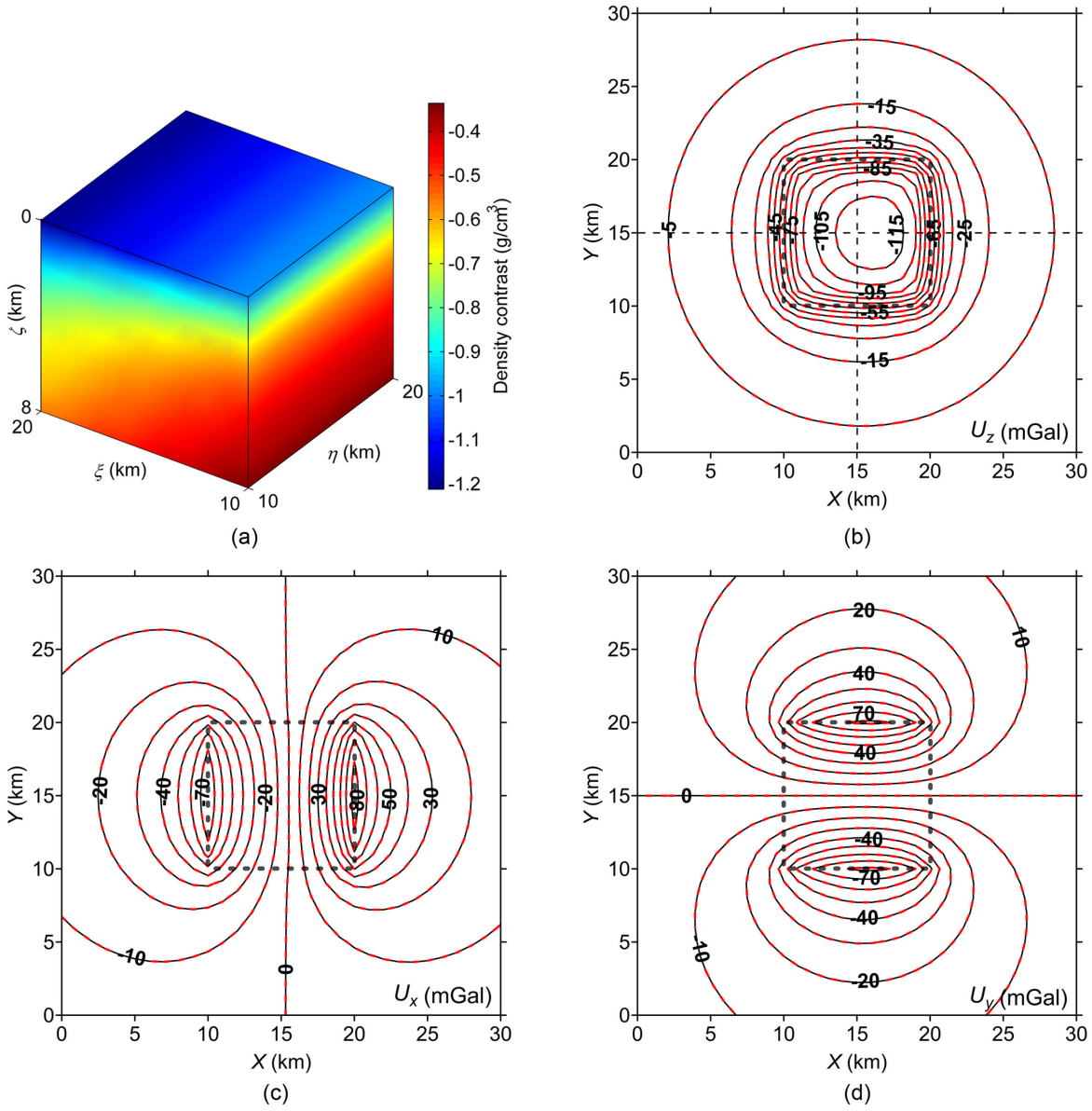

Figure 6. Gravitational vector field of the prism with the density-contrast variation in depth and ξ-direction, given by eq. (55). (a) Prism model, (b) vertical component U_z, (c) x-component U_x and (d) y-component U_y. Solid lines indicate the field computed using the expressions proposed in this paper, and red dashed ones indicate that using the method based on the stack of 560 uniform subprisms. The dotted rectangles indicate the projection of the edges of the prism on the computation plane.

3.3 Error analysis

Holstein & Ketteridge (1996) presented that analytical expressions for gravitational anomalies are often subject to numerical error caused by computer floating point precision in numerical computations. The numerical error increases with increasing of the distance from a computation point to a mass body, while the anomaly decreases. They defined a dimensionless target distance as the ratio of the typical distance between a computation point and a mass body to the linear dimension of the mass body. A critical target distance, being the dimensionless target distance at which the computation error equals to the gravitational value, is used to indicate the limited range of the numerical stability. Beyond the critical target distance, the computation results are dominated by the accumulated round-off error. Here, we test the susceptibility of our analytical expressions derived in this paper to numerical round-off error.

We do tests using the prism model shown in Fig. 2(a). The computation points are located on a line whose coordinates satisfy $X_p = Y_p = Z_p$. All the computations are executed with the double precision. We compute the gravitational anomaly U_z of the prism model with the density-contrast function of depth in eq. (54) using, respectively, our expressions and the method based on the stack of 100 uniform subprisms. Fig. 8(a) shows the two computed anomalies versus the dimensionless target distance. In the range of the target distance from 0 to 90, the two anomalies match well, with a small root-mean-square error (i.e. 3.2697×10^{-5} mGal) between them. Beyond the range, our

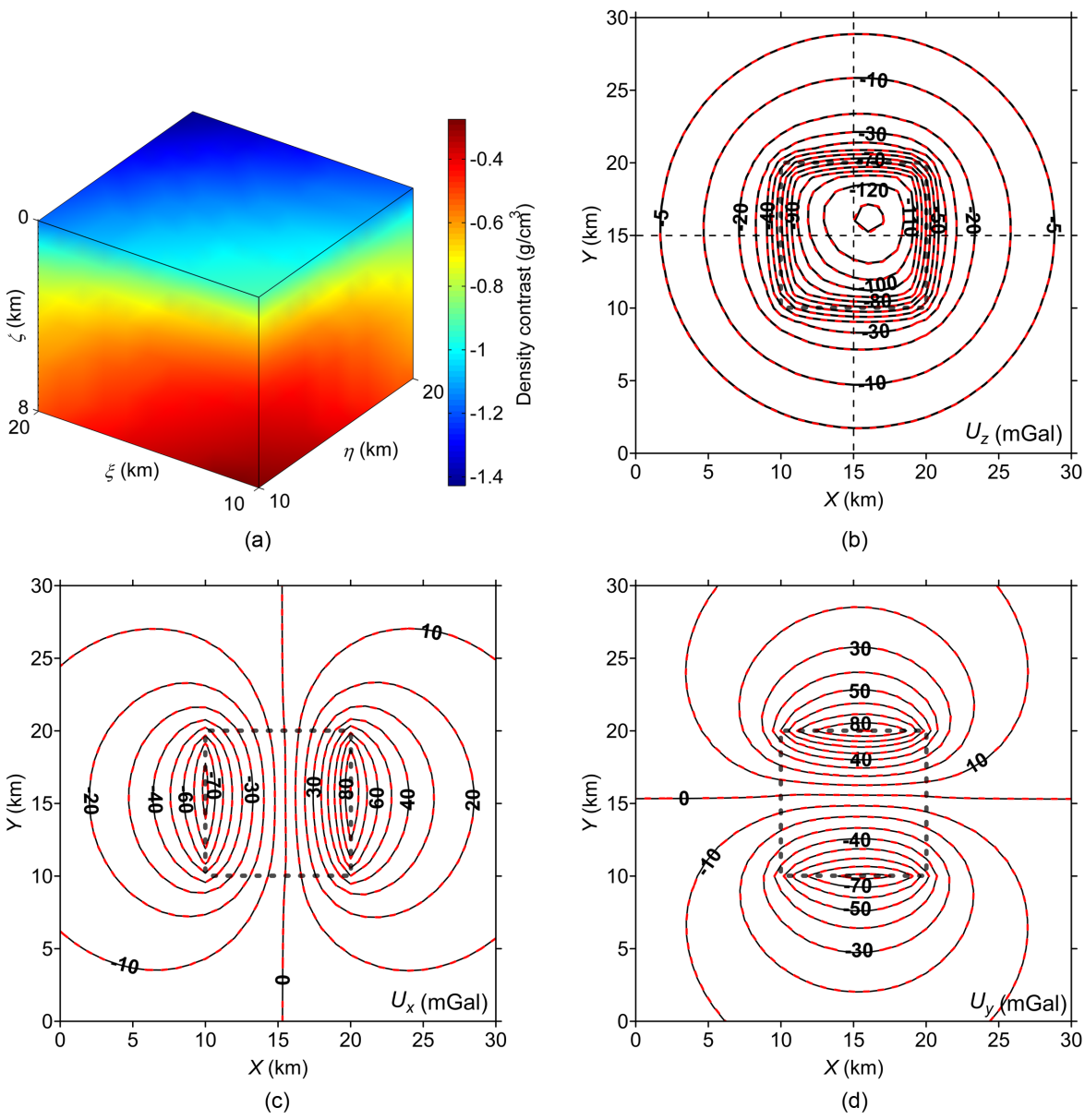

Figure 7. Gravitational vector field of the prism with the density-contrast variation in all three directions given by eq. (56). (a) Prism model, (b) vertical component U_z, (c) x-component U_x and (d) y-component U_y. Solid lines indicate the field computed using the expressions proposed in this paper, and red dashed ones indicate that using the method based on the stack of 3000 uniform subprisms. The dotted rectangles indicate the projection of the edges of the prism on the computation plane.

analytic expressions are instable numerically. The method based on the stack of uniform subprisms is numerically stable within the whole computation-point range, and the field computed using it is then taken as a reference to estimate the error of our expressions. Fig. 8(b) plots the logarithm to base 10 of the relative error against dimensionless target distance for our expressions. The horizontal dashed line indicates the 100 per cent relative error. From Fig. 8(b), the critical target distance of our expressions for U_z is about 110. In this way, the estimated critical target distances are, respectively, 115, 115 and 110 for U_x, U_y and U_z with the density-contrast function of depth in eq. (54), and 135, 132 and 122 for U_x, U_y and U_z with the density-contrast function of the three coordinate directions in eq. (56).

To understand the numerical stability of our expressions for a model with different order polynomial density functions (Case 1 in Table 2), we establish first- to third-order polynomial density-contrast functions of depth for the prism model by fitting density-contrast function in eq. (54) using the least-squares method, listed as follows:

$$\Delta\rho_1(\zeta) = -0.6211 + 7.3024 \times 10^{-5}\zeta,$$

$$\Delta\rho_2(\zeta) = -0.7178 + 1.5036 \times 10^{-4}\zeta - 9.6676 \times 10^{-9}\zeta^2,$$

$$\Delta\rho_3(\zeta) = -0.7477 + 2.0343 \times 10^{-4}\zeta - 2.6764 \times 10^{-8}\zeta^2 + 1.4247 \times 10^{-12}\zeta^3, \quad (57)$$

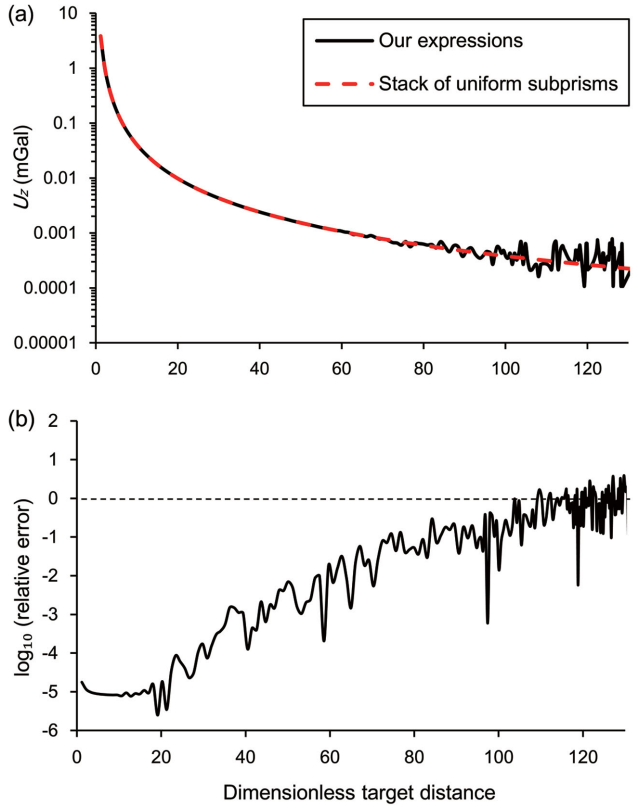

Figure 8. (a) Gravitational anomalies, U_z, of the prism model, shown in Fig. 2(a), with the density-contrast function of depth in eq. (54), computed, respectively, using our expressions and the method based on the stack of 100 uniform subprisms. (b) Logarithm of the relative error against dimensionless target distance for our expressions. The horizontal dashed line indicates the 100 per cent relative error.

Table 2. Critical target distances of our expressions for U_z with different order polynomial density-contrast functions.

Order of density polynomial		1	2	3	4	5	6
Critical target distance	Case 1	1630	340	110			
	Case 2	1480	290	105	48	27	17

where ζ is in metres and density contrast is in g cm^{-3}. The estimated critical target distance for U_z with the different order of polynomial density-contrast functions are listed in the middle row of Table 2. When the order of the density-contrast function increases from 1 to 3, the critical target distance decreases from 1630 to 110, namely, the range of the numerical stability decreases.

In order to understand the effects of high-order variables in a density-contrast function on the critical target distances (Case 2 in Table 2), we assign the density-contrast function in eq. (5) with $a_i = 1$ ($i = 1, \ldots, n$) adopted by Zhou (2010) to the prism model. The estimated critical target distances for U_z with first- to sixth-order polynomial functions are listed in the third row of Table 2. It shows that when the order of the polynomial density-contrast function increases from 1 to 6, the critical target distance decreases from 1480 to 17. With such sixth-order density polynomial, the numerical stability range of our analytic expressions for U_z is from the prism centre about 276 km (17 times the linear dimension of the prism). For the same order in Table 2, the critical target distance in Case 1 is large than that in Case 2.

From above test results, we can conclude that the numerical stability range of our expressions with high-order polynomial density-contrast function is always enough for practical application.

4 CONCLUSIONS

Analytical expressions in a closed-form are proposed for computing the gravitational vector field of a 3-D rectangular prism with density varying as an arbitrary-order polynomial function in one coordinate direction or as a linear combination of arbitrary-order polynomial functions in the three coordinate directions. The expressions not only generalize the existing space-domain analytical solutions for the constant density and low-order polynomial density functions (e.g. zero to third orders), but also have good applicability for arbitrary density functions because of the flexibility of a general polynomial function in approximating arbitrary function variation. Moreover, the expressions can accommodate

to bodies with irregular shape and complex density variation (including multiple sedimentary layers) by using the prisms as building blocks with different polynomial density function per prism, or piecewise-polynomial density functions.

The test examples demonstrate that the expressions have far superiority over the common method based on the stack of uniform subprisms in terms of computational cost. On the other hand, under a certain amount of computer time the expressions within their range of numerical stability have higher accuracy than the common method. Analytical expressions often suffer from numerical error caused by the computer floating point precision. The higher the order of the polynomial density function is, the smaller the range of numerical stability of the expressions is. Generally, our expressions with high-order polynomial density-contrast function have a sufficient range of numerical stability for practical application. Therefore, the expressions offer an effective approach to compute the gravitational vector field from 3-D bodies with irregular shape and variable density.

ACKNOWLEDGEMENTS

We sincerely thank the editors Prof Jörg Renner and Dr Bert Vermeersen, reviewers Prof Dimitrios Tsoulis, Prof Gábor Papp and his colleague Dr Judit Benedek and two anonymous reviewers for their constructive comments and suggestions which significantly improve this paper. This work was supported by the National Natural Science Foundation of China (grant nos 41074077 and 41230318), and the Specialized Research Fund for the Doctoral Program of Higher Education (grant no. 20130132110023).

REFERENCES

Banerjee, B. & Das Gupta, S.P., 1977. Gravitational attraction of a rectangular parallelepiped, *Geophysics*, **42**, 1053–1055.

Chai, Y. & Hinze, W.G., 1988. Gravity inversion of an interface above which the density contrast varies exponentially with depth, *Geophysics*, **53**, 837–845.

Chakravarthi, V., Raghuram, H.M. & Singh, S.B., 2002. 3-D forward gravity modeling of basement interfaces above which the density contrast varies continuously with depth, *Comput. Geosci.*, **28**, 53–57.

D'Urso, M.G., 2015. The gravity anomaly of a 2D polygonal body having density contrast given by polynomial functions, *Surv. Geophys.*, **36**, 391–425.

Gallardo-Delgado, L.A., Pérez-Flores, M.A. & Gómez-Treviño, E., 2003. A versatile algorithm for joint 3D inversion of gravity and magnetic data, *Geophysics*, **68**, 949–959.

García-Abdeslem, J., 1992. Gravitational attraction of a rectangular prism with depth-dependent density, *Geophysics*, **57**, 470–473.

García-Abdeslem, J., 2005. The gravitational attraction of a right rectangular prism with density varying with depth following a cubic polynomial, *Geophysics*, **70**, J39–J42.

Holstein, H. & Ketteridge, B., 1996. Gravimetric analysis of uniform polyhedral, *Geophysics*, **61**, 357–364.

LaFehr, T.R. & Nabighian, M.N., 2012. *Fundamentals of Gravity Exploration*, Society of Exploration Geophysicists, doi:10.1190/1.9781560803058.

Li, X., 2001. Vertical resolution: gravity versus vertical gravity gradient, *Leading Edge*, **20**, 901–904.

Li, X. & Chouteau, M., 1998. Three-dimensional gravity modeling in all space, *Sur. Geophys.*, **19**, 339–368.

Mollweide, K.B., 1813. Auflösung einiger die Anziehing von Linien Flächen und Köpern betreffenden Aufgaben unter denen auch die in der Monatl Corresp Bd XXIV. S. 522. vorgelegte sich findet. Zach's Monatliche Correspondenz zur Beförderung der Erd- und Himmelskunde, Bd XXVII, pp. 26–38.

Nagy, D., 1966. The gravitational attraction of a right rectangular prism, *Geophysics*, **31**, 362–371.

Nagy, D., Papp, G. & Benedek, J., 2000. The gravitational potential and its derivatives for the prism, *J. Geod.*, **74**, 552–560.

Papp, G. & Kalmar, J., 1995. Investigation of sediment compaction in the Pannonian basin using 3D gravity modelling, *Phys. Earth planet. Inter.*, **88**, 89–100.

Tsoulis, D. & Petrović, S., 2001. On the singularities of the gravity field of a homogeneous polyhedral body, *Geophysics*, **66**, 535–539.

Verweij, J.M., Boxem, T.A.P. & Nelskamp, S., 2016. 3D spatial variation in vertical stress in on- and offshore Netherlands: integration of density log measurements and basin modeling results, *Mar. Petrol. Geol.*, **78**, 870–882.

Wu, L. & Chen, L., 2016. Fourier forward modeling of vector and tensor gravity fields due to prismatic bodies with variable density contrast, *Geophysics*, **81**, G13–G26.

Zhang, J., Zhong, B., Zhou, X. & Dai, Y., 2001. Gravity anomalies of 2D bodies with variable density contrast, *Geophysics*, **66**, 809–813.

Zhou, X., 2009. 3D vector gravity potential and line integrals for the gravity anomaly of a rectangular prism with 3D variable density contrast, *Geophysics*, **74**, I43–I53.

Zhou, X., 2010. Analytical solution of the gravity anomaly of irregular 2D masses with density contrast varying as a 2D polynomial function, *Geophysics*, **75**, I11–I19.

Zwillinger, D., 2003. *CRC Standard Mathematical Tables and Formulae*, 31st edn, CRC Press.

APPENDIX: SOLUTIONS OF SOME INDEFINITE INTEGRALS

Here, we list several indefinite integral solutions used in the derivation of the analytical expressions in the text body above, in which the integral constants are omitted. The notations are the same as those in the text body.

Following eqs (6)–(9) of García-Abdeslem (1992), we have

$$\int \frac{1}{(y^2+z^2)r}dy = \frac{1}{xz}\arctan\frac{xy}{zr}. \tag{A1}$$

Applying formulae (20), (131), (141) and (183) in the table of indefinite integrals of Zwillinger (2003), we have

$$\int \frac{1}{r} dz = \ln(z + r), \tag{A2}$$

$$\int \frac{(x^2 + z^2)^{k-1}}{r} dz^2 = 2(-1)^{k-1} y^{2(k-1)} r \sum_{l=0}^{k-1} \frac{(-1)^l (k-1)! r^{2l}}{(2l+1) l! (k-l-1)! y^{2l}}, \tag{A3}$$

$$\int \frac{1}{(x^2 + z^2) r} dz^2 = \frac{2}{y} \left[\ln \sqrt{x^2 + z^2} - \ln(y + r) \right], \tag{A4}$$

$$\int \frac{z^{2l}}{r} dz = \frac{(-1)^l (2l)! (x^2 + y^2)^l}{2^{2l} (l!)^2} \left[\ln(z + r) + r \sum_{q=1}^{l} \frac{(-1)^q 2^{2q-1} q! (q-1)! z^{2q-1}}{(2q)! (x^2 + y^2)^q} \right]. \tag{A5}$$